Analysis of Nanopore Structure Images Using MATLAB Software

Article *in* Eurasian Journal of Science and Engineering · January 2019

DOI: 10.23918/eajse.v4i3sip84

CITATIONS
3

READS
465

3 authors:

Haidar Jalal Ismail
Salahaddin University - Erbil
24 PUBLICATIONS **54** CITATIONS
SEE PROFILE

Azeez Abdullah Barzinjy
Soran University
157 PUBLICATIONS **2,027** CITATIONS
SEE PROFILE

Samir Hamad
Soran University
101 PUBLICATIONS **1,385** CITATIONS
SEE PROFILE

Analysis of Nanopore Structure Images Using MATLAB Software

Haidar Jalal Ismail[1] & Azeez Abdullah Barzinjy[1,2] & Samir Mustafa Hamad[3,4]

[1]Department of Physics, College of Education, Salahaddin University, Erbil, Iraq
[2]Department of Physics Education, Faculty of Education, Ishik University, Erbil, Iraq
[3]Research centre, Cihan University, Erbil, Iraq
[4]Scientific Research Centre, Delzyan Campus, Soran University, Iraq
Correspondence: Haidar Jalal Ismail, Salahaddin University, Erbil, Iraq.
Email: haidar.ismail@su.edu.krd

Received: October 25, 2018 Accepted: December 20, 2018 Online Published: January 1, 2019

doi: 10.23918/eajse.v4i3sip84

Abstract: The importance of nanopores increases with time due to their application. For instance, nanopores may be used to sense molecules like DNA and RNA, single proteins, etc. Sequencing by nanopore has also a possibility to be a direct, fast, and inexpensive DNA sequencing tool. Diameters of nanopores are the main keys for mentioned sensing processes. Three segmenting methods used in this study namely Thresholding, Gaussian Mixture Model-Expectation Maximization (GMM-EM) and Hidden Markov Random Field-Expectation Maximization (HMRF-EM). These methods applied on three SEM nanopore images after enhancing them through obtaining optimum parameters of CLAHE contrast-enhanced method to give high PSNR. The results of the Rand index and time of running code show that the HMRF-EM is better than GMM-EM. Hence, their segmented images are used to find out nanopore parameters including total counting pores, diameter, and porosity. The results of porosity were in good agreement with former investigations. Consequently, the HMRF-EM segmenting technique with procedures utilized in this study using image processing for finding porosity gives promising results among other examined methods.

Keywords: Nanopore, Image Segmentation, Segmentation Evaluation, GMM-EM, HMRF-EM

1. Introduction

One of the essential requests of nanopores is in detecting unlabeled biopolymers like RNA, DNA, and single proteins. The sensing took place when the current reduced for passing molecules across nanopore (Raillon, Granjon, Graf, Steinbock, & Radenovic, 2012). So, the knowledge of nanopore diameter is so essential for determination of the size of molecules passed across it. The diameter may be computed through applying image processing methods on SEM images. Image-segmentation is considered as one of the essential image processing techniques for dividing SEM images to nanopores and interpore regions. Threshold segmenting is a simple technique; with sometimes acceptable results but suffer from long time-consuming due to its working strategy on trial and error method. Akhtaruzzaman *et al.* (2016) made an automatic threshold sensing on video of human walking. The technique was for changing image frames to grayscale images. They used line fill method to smooth edges of the object and remove the background. Another method of segmenting was Expectation Maximization-Gaussian mixture model (EM-GMM). Fu and Wang (2012) applied it on colour images and the results show the aptitude of the technique. The above mentioned and

Fuzzy-C-Means (FCM) methods are used, mostly, in image segmentation. Their drawback was for images with noises. Kalti and Mahjoub (2014) used different methods to overcome this issue. They achieved a technique to increase the specification of the segmented image than the standard version of GMM-EM and FCM. Another segmenting method which is used widely in medical imaging process is Hidden Markov Random Field-Expectation Maximization (HMRF-EM). Sajja *et al.* (2006) used the mentioned technique to solve the issue of a lot of number of false lesion classification which effects in precise finding volumes of multiple sclerosis (MS). The technique provides Contextual information to reduce false negative lesion classification. Nie *et al.* (2009) improve their segmenting results of low-resolution MRI arrangement through their suggested algorism based on locative accuracy-weighted HMRF-EM. Huang *et al.* (2015) used the HMRF-EM process to refine segmenting tumor which acquired using the nearby neighbor display model. Their suggested technique verified on MRI images of 26 nasopharyngeal-carcinoma patients and obtained respectable outcomes.

After segmenting the SEM nanopores the geometrical nanopore structures could be studied. A lot of researchers have studied it. Alexander *et al.* (2009) used Histogram Equalization with the morphological operation to segment nanopores and found their size, perimeter, and other geometric features. Another researcher found the size of nanopores by morphological and Canny edge detection for segmenting SEM images (Phromsuwan, Sirisathitkul, Sirisathitkul, Muneesawang, & Uyyanonvara, 2013). Bannigidad and Vidyasagar (2015) obtained diameter and statistical features of nanopores by global thresholding and morphological operation. All the above methods based on trial and error strategy to properly segmenting nanopores (Vidyasagar, Bannigidad, & Muralidhara, 2016). Ismail *et al.* (2017) used threshold, bilateral filter, kmeans, GMM-EM segmenting techniques which applied on SEM images with nanopore structure and found that GMM-EM segmenting method gives hopeful results among other examined methods.

This study investigates the quality of segmenting nanopores in SEM images by using GMM-EM and HMRF-EM. The geometrical parameters, such as diameter, count, and porosity, will be computed according to better segmenting techniques used here.

2. Material and Methods

Three SEM micrographs for aluminum-sulfuric acid, Al-Sf, aluminum-oxalic acid, Al-Ox/SiO_2, and the commercial anopore membrane samples used in this study are taken from Romero *et al.* (2014). They cropped to get free of labels and scale bars that effect segmenting and counting procedures which applied in this study. The images enhanced by Contrast Limited Adaptive Histogram Equalization (CLAHE), which is well-known and efficient contrast-enhanced technique. The related parameters optimized for all SEM images to get the highest possible peak signal to noise ratio. The Peak Signal to Noise Ratio (PSNR) is a parameter used to measure image qualities.

The images are segmented through three techniques. The Threshold segmenting used to get ground truth images of pores that are necessary to evaluate Rand index parameter. The mentioned parameter is used to compute the segmentation efficiently. Another two techniques of segmentation used here were the Gaussian Mixture Model - Expectancy Maximization (GMM-EM) and Hidden-Markov-Random-Field Model-Expectation Maximization (HMRF-EM). The mentioned three techniques are explained in some detail as following.

2.1 Segmenting Techniques

2.1.1 Thresholding

Thresholding is a technique of selecting the optimum grey-level value which separates the region of interest from other regions. Thresholding produced binary images from grey-level images by making pixels lower or greater than a grey-level value to zero and other remaining pixels to one. If g(x, y) is the doorstep output of an input f(x, y) at specific input grey-level value T, it might be described as (Vala & Baxi, 2013),

$$g(x,y) = \begin{cases} 1 & f(x,y) > T \\ 0 & otherwise \end{cases} \quad (1)$$

2.1.2 GMM-EM

The Gaussian mixture model consists of Gaussian distributions that defined as,

$$f(x_n) = \sum_{k=1}^{K} \pi_k N(x_n|\Theta_k) \quad (2)$$

where every component of function $N(x_n|\Theta_k)$ is a Gaussian distribution and for a D-dimensional vector x, defined as,

$$N(x|\Theta) = \frac{1}{(2\pi)^{D/2}} \frac{1}{|\Sigma|^{1/2}} \; exp\left\{-\frac{1}{2}(x - \mu)^T \Sigma^{-1}(x - \mu)\right\} \quad (3)$$

where μ and Σ are the D-dimensional average vector and a D×D covariance-matrix, respectively. The prior distribution π_k is the probability of noticing x_n that belong to the k^{th} class Ω_k. It is unrelated to the observation x_n. Moreover, π_k must possess these restrictions:

$$0 \leq \pi_k \leq 1 \, , \sum_{k=1}^{K} \pi_k \; ; \; k = 1, \dots, K \quad (4)$$

After finding the density function for a remark, the log-likelihood function of N interpretations is,

$$L(\Theta) = \sum_{n=1}^{N} \log(\sum_{k=1}^{K} \pi_k N(x_n|\Theta_k) \quad (5)$$

According to the equations 2 and 5, the major feature of the GMM is that its arrangement is too straightforward within few variables. Moreover, when GMM is used in image segmentation, the correct results are obtained if they unrelated to each other. To find the variables (π_k, μ_k, Σ_k), the Expectation-Maximization (EM) step is usually applied to get upper limit of the log-likelihood function in equation 5. The last probability for expectation stage of EM is obtained as,

$$p^t(\Theta_k|x_n) = \frac{\pi_k N(x_n|\Theta_k)}{\sum_{j=1}^{K} \pi_j N(x_n|\Theta_j)} \quad (6)$$

In the maximization stage of EM, the parameters (π_k, μ_k, Σ_k) are changed iteratively through the following formulas,

$$\mu_k^{t+1} = \frac{\sum_{n=1}^{N} p^t(\Theta_k|x_n) X_n}{\sum_{n=1}^{N} p^t(\Theta_k|x_n)} \quad (7)$$

$$\Sigma_k^{t+1} = \frac{\sum_{n=1}^{N} p^t(\Theta_k|x_n)(x_n-\mu_k)(x_n-\mu_k)^T}{\sum_{n=1}^{N} p^t(\Theta_k|x_n)} \pi_k^{t+1} = \frac{\sum_{n=1}^{N} p^t(\Theta_k|x_n)}{N} \quad (8)$$

where *t* indicates the repetition value. The circlet is stopped in the accumulation condition. The value from equation 5 for maximum posterior criterion used to get the class label for each pixel (Xiong, Zhang, & Yi, 2016).

2.1.3 HMRF-EM

For simplicity, first presumed that the graphs are 2D grey-level, and the intensity-distribution for any area to be segmented follows a Gaussian distribution. Given an image Y = (y_1,...,y_N) where N is the number of pixels and any y_i is the grey-level intensity of a pixel. A configuration inferred to marks X = (x_1,...,x_N) where $x_i \in$ L and L include set of whole possible labels. In a binary-segmentation case, L = [0,1]. As claimed by the MAP criterion, the labelling X^x sought to satisfies (Abdulbaqi, Jafri, Omar, Mustafa, & Abood, 2015; Wang, 2012),

$$X^x = argmax\{P(Y|X,\theta), P(X)\} \quad (9)$$

where, P(X) is the Gibbs distribution and the joint likelihood probability is,

$$P(Y|X, \theta) = \Pi_i P(y_i|X,\theta) = \Pi_i P(y_i|x_i,\theta_{xi}) \quad (10)$$

where P(yi|xi; Θ_{xi}) is a Gaussian-distribution with factors $\theta_{xi} = (\mu_{xi},\sigma_{xi})$.
Expectation maximization is done to minimize the likelihood function for all parameters including the means and covariance of the components and the mixing coefficient. One can obtain $\theta^{(t)}$ by assuming an initial parameter $\theta^{(0)}$ at the i^{th} iteration by,

$$Q\left(\theta\middle|\theta^{(t)}\right) = \sum_{X\in x} P\left(X\middle|Y,\theta^{(t)}\right) \ln P(X,Y|\theta) \quad (11)$$

where x is a set of possible configuration of labels. The equation 11 maximized to obtain next estimate (M-step),

$$\theta^{(t+1)} = \text{argmax}_\theta\, Q\left(\theta\middle|\theta^{(t)}\right) \quad (12)$$

Now set $\theta^{(t+1)}$ to $\theta^{(t)}$ and find new $^{(t+1)}$ by repeating from the equation 11. Let G (z,) denote a Gaussian distribution function with parameters θ_l=(μ_l,σ_l),

$$G(z,\theta_l) = \frac{1}{\sqrt{2\pi\sigma_l^2}} e^{-\frac{(z-\mu_l)^2}{2\sigma_l^2}} \quad (13)$$

Assume prior probability as,

$$P(X) = \frac{1}{z} e^{-U(X)} \quad (14)$$

where U(X) is the beforehand energy-function. Presuming that,

$$P(Y|X,\theta) = \frac{1}{z} e^{-U(Y|X)} \quad (15)$$

From these assumptions, HMRF-EM algorithm can be applied by setting initial parameter $^{(0)}$ and evaluating the likelihood distribution $P^{(t)}(y_i|x_i,\theta_{xi})$. So, from current parameter $^{(t)}$, the labels can be estimated through MAP assessment,

$$X^{(t)} = \text{argmin}_{X\in x}\{U(Y|X,\theta^{(t)}) + U(X)\} \quad (16)$$

Baye's rule can be used in evaluating the subsequent dissemination for entire element of L and whole pixels y_i,

$$P^{(t)}(l|y_i) = \frac{G(y_i,\theta_l)\,P(l|x_{Ni}^{(t)})}{P^{(t)}y_i} \quad (17)$$

where $x_{Ni}^{(t)}$ is the neighbourhood configuration of $x_i^{(t)}$,

$$P^{(t)}y_i = \sum_{l\in L} G(y_i,\theta_l)\,P(l|x_{Ni}^{(t)}) \quad (18)$$

$$P\left(l\middle|x_{Ni}^{(t)}\right) = \frac{1}{z}e^{-\sum_{j\in Ni} Vc(l,x_t^{(t)})} \quad (19)$$

So, Eq. 17 applied to update the parameters,

$$\mu_l^{(t+1)} = \frac{\sum_i P^{(t)}(l|y_i)y_i}{\sum_i P^{(t)}(l|y_i)} \quad (20)$$

$$\left(\sigma_l^{(t+1)}\right)^2 = \frac{\sum_i P^{(t)}(l|y_i)\left(y_i-\mu_l^{(t+1)}\right)^2}{\sum_i P^{(t)}(l|y_i)} \quad (21)$$

The MAP estimation mentioned above is a mode of the posterior distribution. It can work as a regularization of maximum likelihood (ML) estimation. In the EM algorithm, X^X solved to minimize, equation 16, through the assumed Y and θ, and for the likelihood energy,

$$U(Y|X,\theta) = \sum_i\left[\frac{(y_i-\mu_{xi})^2}{2\sigma_{xi}^2} + \ln\sigma_{xi}\right] \quad (22)$$

The prior energy-function is,

$$U(X) = \sum_{c\in C} V_C(X) \quad (23)$$

where $V_C(X)$ is the set potential and c is the set of all likely cliques. Each pixel has four neighbours, then clique potential for pixel is well-defined as,

$$V_C(x_i,x_j) = \frac{1}{2}(1 - I_{xi,xj}) \quad (24)$$

where,

$$I_{xi,xj} = \begin{cases} 0 & if\ xi \neq xj \\ 1 & if\ \ xi = xj \end{cases} \quad (25)$$

So, there is an iterative algorithm to solve equation 16.

a. Rand Index

The Rand index, founded by William Rand (1971), utilized for the comparison of two arbitrary segmentations using pair-wise label relationships. It is obtained by division of the number of pixel pairs that have the same label relationship in both segmentations. The n_{uv} is the amount of points labelled *u* in S and that labelled *v* in S'. The labelled points *u* in the leading part of S, labelled points *v* in second part S', is termed $n_{u\blacksquare}$ and $n_{\blacksquare v}$, respectively. Afterward,

$$n_{u\blacksquare} = \sum_v n_{uv}\, n_{\blacksquare v} = \sum_u n_{uv} \quad (26)$$

Clearly $\sum_u \boldsymbol{n_{u\blacksquare}} = \sum_v \boldsymbol{n_{\blacksquare v}} = \boldsymbol{N}$ is the entire numbers of points. So, the Rand index is,

$$R(S,S') = 1 - \frac{\frac{1}{2}\left(\sum_u n_{u\blacksquare}^2 + \sum_v n_{u\blacksquare}^2\right) - \sum_{u,v} n_{uv}^2}{N(N-1)/2} \quad (27)$$

The R-index is 1 when both segmentations have total similarities and 0 for zero ones. This type of similarity measurements takes small running time when exclusive labels in S and S' are slighter than the total data numbers N (Unnikrishnan & Hebert, 2005).

b. Porosity

Porosity can be computed through using the area of the pores A_p and the total area A_t by,

$$P_a = \frac{A_p}{A_t} \times 100 \quad (28)$$

Also, it can be obtained using pore diameter (D_p) and interpore distance (D_{int}) (as shown in the Figure 1), for homogeneous uniformed pores on ordered-structured hexagons, as (Zhao *et al.*, 2017),

$$P_d = \frac{\pi}{2\sqrt{3}}\left(\frac{D_p}{D_{int}}\right)^2 \times 100 \quad (29)$$

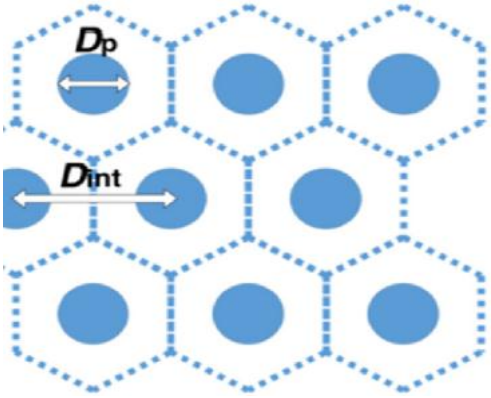

Figure 1: Illustration of pore diameter and interpore distance

In this work, average pore diameter is computed, and interpore distance is founded through using the

following formula,

$$D_p = \frac{6\,A_b}{360\,t} \tag{30}$$

where A_b and t are total background area and total pore count, respectively. Number 6, in the above equation, is an indicator for the corporation of each pore with six surrounding nanopores and 360 for obtaining the line between one nanopore and its neighbour.

3. Results and Discussion

The three SEM images that cropped, for getting free of label and scale bars, were enhanced to a well-known and good contrast enhancing technique that called CLAHE. Optimum PSNR values found from them are 103.7, 59.8 and 65.8 for A, B, and C (see Figure 2), respectively. The images are segmented by using three techniques. Threshold segmenting is used to get ground truth image that is necessary for obtaining the Rand Index. It neglected for computing porosity due to large attempt to get better segmenting and their large time to obtain it (as shown in the second row of Figure 2).

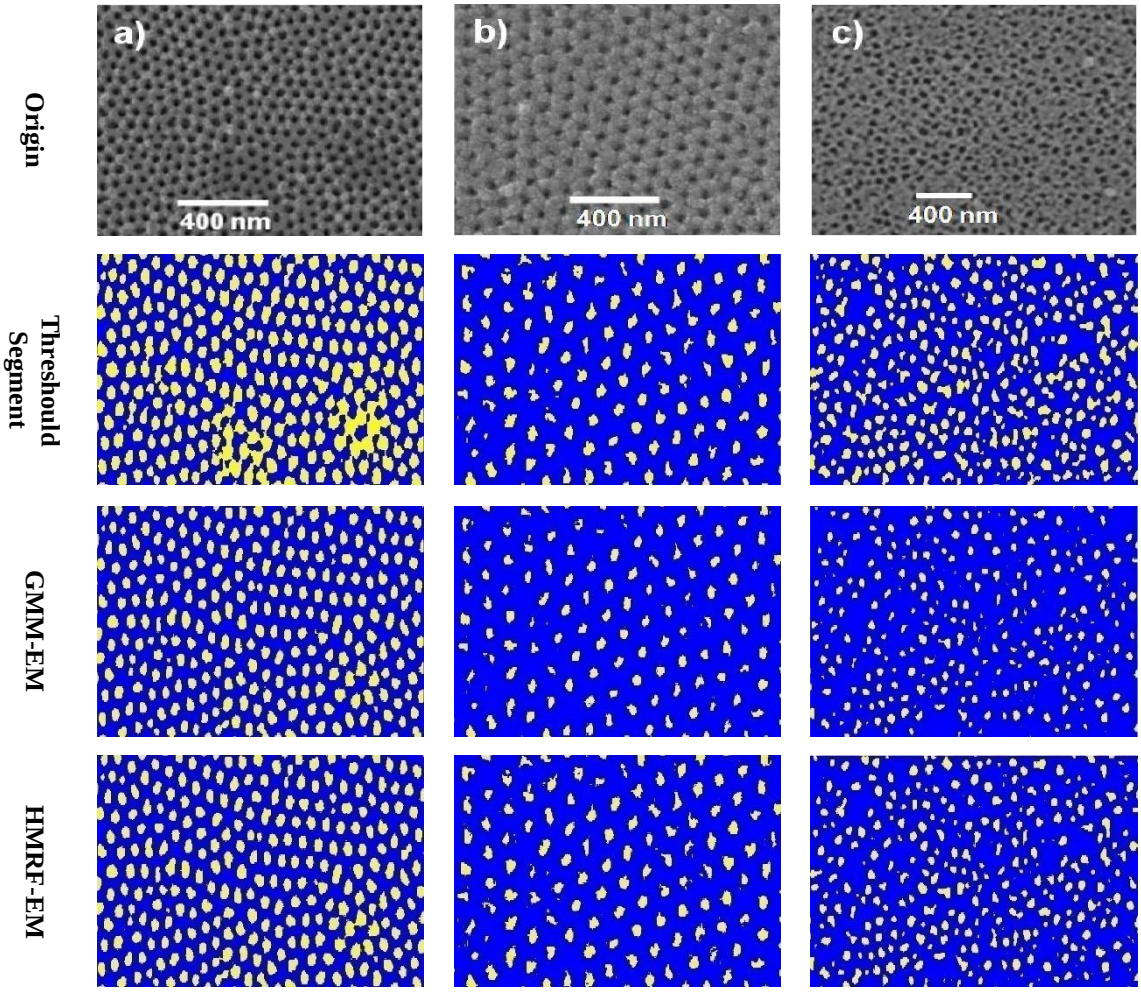

Figure 2: Shows three segmentation methods for three SEM images with scale bar 400 nm (Romero *et al*., 2014).

Figure 2 shows the results of the threshold, GMM-EM, and HMRF-EM segmenting techniques on all

three SEM nanopore images. The Rand index and time of running are listed in Table 1. It can be noticed that HMRF-EM possesses superior representation for all three samples than the GMM-EM through comparing their values of Rand Index. Also, the time of running is smaller than GMM-EM. In the previous work, Ismail *et al.* (2017) founded that GMM-EM was better than kmeans and bilateral filter for segmenting similar SEM nanopore images. But, according to the results of this work, HMRF-EM segmenting techniques provide better performance and smaller time of running. So, the results of HMRF-EM are used in following steps of counting and computing porosity.

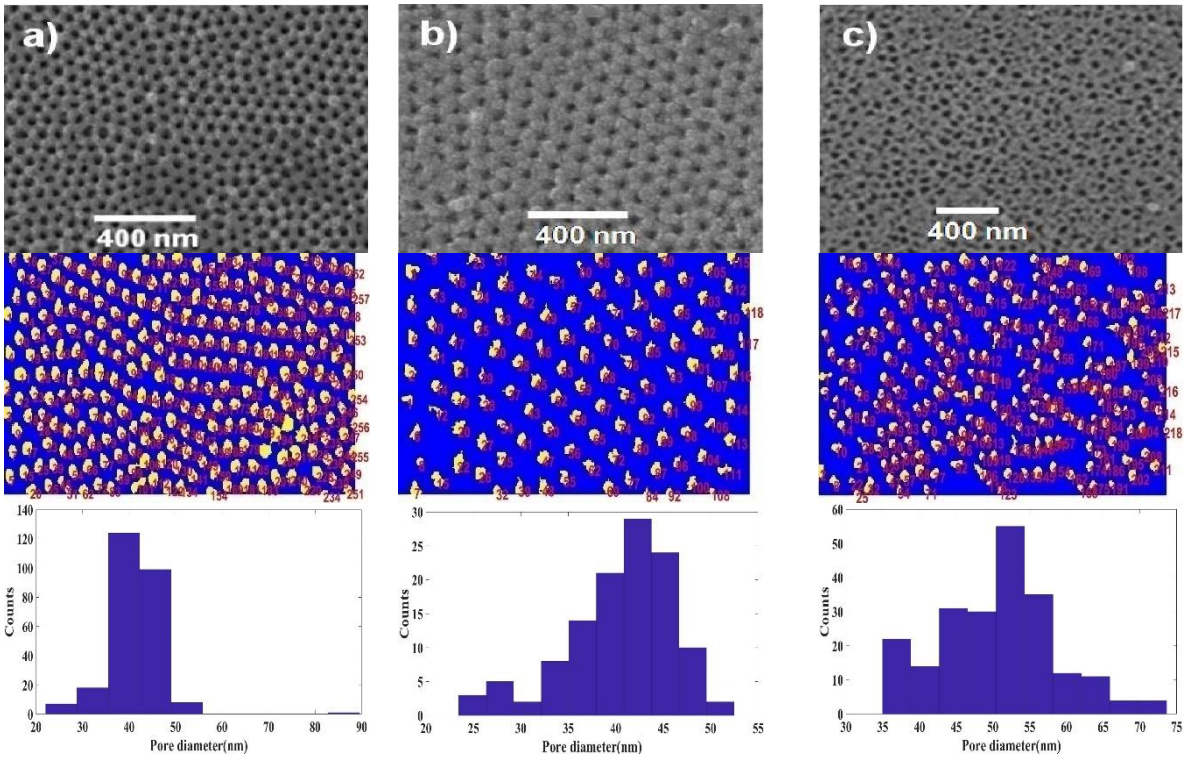

Figure 3: Shows total counting nanopores (second row), and histogram distribution of nanopore diameters (third row) for HMRF-EM segmenting techniques, that has higher Rand index than GMM-EM, for all three SEM types.

Figure 3 shows counting nanopores for all SEM image (second row) and distribution of nanopore diameter values through histogram chart (third row). The standard deviation values of nanopore diameters are large due to some variations of the diameter as seen in histogram diameter of Figure 3.

Table 1: Time-consuming, Rand index, nanopore diameter and nanopore counts for all SEM images segmented by GMM-EM and HMRF-EM techniques

Nanopores	A		B		C	
	GMM-EM	HMRF-EM	GMM-EM	HMRF-EM	GMM-EM	HMRF-EM
Time(s)	20.98	10.82	20.96	10.19	20.40	11.72
Rand index	0.82	0.84	0.93	0.98	0.78	0.87
Total Pore	-	257	-	118	-	218
Pore Diameter(nm)	-	41.7±2	-	40.99±2	-	51.46±2
Interpore distance(nm)	-	98.6	-	201.6	-	265.4
Porosity (Area method)	-	% 28.7	-	% 12.1	-	% 14.0
Porosity (Pore diameter method)	-	% 16.2	-	% 3.86	-	% 7.0
Porosity (Romero *et al.*, 2014)	-	% 15	-	% 5	-	% 5

There is some deviation between the two methods of computing porosity as seen in Table 1. But, the results of porosity are similar to what are found in research that SEM images are taken from it (Romero *et al.*, 2014). The mentioned research uses SEM micrographs analysis.

4. Conclusions

In this study, three segmenting methods were applied to three SEM images with different components. The threshold segmenting may give acceptable results, as used commonly, but suffer from request a large number of trial and error to get optimum results. So, it was used here just as ground truth images. In comparison between GMM-EM and HMRF-EM, one found that the later is better for its higher Rand index and smaller time of running. The results of computing porosity are acceptable in comparison to other works. Accordingly, HMRF-EM with the method of counting, diameter founding, and porosity computation can be used efficiently for SEM images.

Acknowledgements

Firstly, the authors would like to thank Almighty Allah for substantial skill, sympathetic, skills and chance to finish this study efficiently. Without Allah's supports, this achievement would not have been probable. They would also like to direct their gratitude to the Soran research Centre, Salahaddin and Ishik University for their facility and entrance fee to obtainable implements. Please contact the corresponding author for any further assistance regarding the MATLAB codes. This study is partially supported by Ishik University Research Center.

References

Abdulbaqi, H. S., Jafri, M. Z. M., Omar, A. F., Mustafa, I. S. B., & Abood, L. K. (2015). *Detecting brain tumor in computed tomography images using Markov random fields and fuzzy C-means clustering techniques.* Paper presented at the AIP Conference Proceedings.

Akhtaruzzaman, M., Shafie, A. A., & Khan, M. R. (2016). Automated Threshold Detection for Object Segmentation in Colour Image. *ARPN Journal of Engineering and Applied Sciences, Asian Research Publishing Network (ARPN), 11*(6), 4100-4104.

Alexander, S., Azencott, R., Bodmann, B. G., Bouamrani, A., Chiappini, C., Ferrari, M., . . .

Tasciotti, E. (2009). *SEM image analysis for quality control of nanoparticles.* Paper presented at the International Conference on Computer Analysis of Images and Patterns.

Bannigidad, P., & Vidyasagar, C. (2015). Effect of time on anodized Al2O3 nanopore FESEM images using digital image processing techniques: A study on computational chemistry. *International Journal of Emerging Trends and Technology in Computer Science (IJETTCS), 4*(3), 15-22.

Fu, Z., & Wang, L. (2012). *Color Image Segmentation Using Gaussian Mixture Model and EM Algorithm*, Berlin, Heidelberg.

Huang, K.-W., Zhao, Z.-Y., Gong, Q., Zha, J., Chen, L., & Yang, R. (2015). *Nasopharyngeal carcinoma segmentation via HMRF-EM with maximum entropy.* Paper presented at the Engineering in Medicine and Biology Society (EMBC), 2015 37th Annual International Conference of the IEEE.

Ismail, H. J., Barzinjy, A. A. A., & Jabbar, K. Q. (2017). Estimation of Nano-Pore Size Using Image Processing. *UHD Journal of Science and Technology, 1*(1), 38-44.

Kalti, K., & Mahjoub, M. A. (2014). Image segmentation by gaussian mixture models and modified FCM algorithm. *Int. Arab J. Inf. Technol., 11*(1), 11-18.

Nie, J., Xue, Z., Liu, T., Young, G. S., Setayesh, K., Guo, L., & Wong, S. T. (2009). Automated brain tumor segmentation using spatial accuracy-weighted hidden Markov Random Field. *Computerized Medical Imaging and Graphics, 33*(6), 431-441.

Phromsuwan, U., Sirisathitkul, Y., Sirisathitkul, C., Muneesawang, P., & Uyyanonvara, B. (2013). Quantitative analysis of X-ray lithographic pores by SEM image processing. *Mapan, 28*(4), 327-333.

Raillon, C., Granjon, P., Graf, M., Steinbock, L., & Radenovic, A. (2012). Fast and automatic processing of multi-level events in nanopore translocation experiments. *Nanoscale, 4*(16), 4916-4924.

Rand, W. M. (1971). Objective criteria for the evaluation of clustering methods. *Journal of the American Statistical Association, 66*(336), 846-850.

Romero, V., Vega, V., García, J., Prida, V. M., Hernando, B., & Benavente, J. (2014). Effect of porosity and concentration polarization on electrolyte diffusive transport parameters through ceramic membranes with similar nanopore size. *Nanomaterials, 4*(3), 700-711.

Sajja, B. R., Datta, S., He, R., Mehta, M., Gupta, R. K., Wolinsky, J. S., & Narayana, P. A. (2006). Unified approach for multiple sclerosis lesion segmentation on brain MRI. *Annals of Biomedical Engineering, 34*(1), 142-151.

Unnikrishnan, R., & Hebert, M. (2005). *Measures of similarity.* Paper presented at the Application of Computer Vision, 2005. WACV/MOTIONS'05 Volume 1. Seventh IEEE Workshops on.

Vala, M. H. J., & Baxi, A. (2013). A review on Otsu image segmentation algorithm. *International Journal of Advanced Research in Computer Engineering & Technology (IJARCET), 2*(2), pp: 387-389.

Vidyasagar, C., Bannigidad, P., & Muralidhara, H. (2016). Influence of anodizing time on porosity of nanopore structures grown on flexible TLC aluminium films and analysis of images using MATLAB software. *Adv. Mater. Lett, 7*(1), 71-77.

Wang, Q. (2012). Gmm-based hidden markov random field for color image and 3d volume segmentation. *arXiv preprint arXiv:1212.4527*.

Xiong, T., Zhang, L., & Yi, Z. (2016). Double Gaussian mixture model for image segmentation with spatial relationships. *Journal of Visual Communication and Image Representation, 34*, 135-145.

Zhao, S., Fan, H., Yin, N., Lin, T., Zhang, S., Xu, X., Zhu, X. (2017). Image binarization to calculate porosity of porous anodic oxides and derivation of porosity vs current. *Materials Research Bulletin, 93*, 138-143.